Materials Transactions, Vol. 65, No. 11 (2024) pp. 1420 to 1430

Effect of Solution Heat Treatment on Dendritic Segregation and Creep Strength of Ni-Base Single Crystal Superalloy TMS-238*1

Tadaharu Yokokawa[1], Toshio Osada[1,*2], Chihiro Tabata[1,2], Takuma Kohata[1], Yuji Takata[1], Michinari Yuyama[1] and Kyoko Kawagishi[1]

[1]*Research Center for Structural Materials, National Institute for Materials Science, Tsukuba 305-0047, Japan*
[2]*Department of Materials Science, School of Fundamental Science and Engineering, Waseda University, Tokyo 169-8555, Japan*

To reduce the cost of solution heat treatment process Ni-base single crystal superalloy TMS-238 containing Re and Ru, quantitative analysis of dendrite-interdendrite segregation of alloying elements under various solution heat treatment conditions were conducted, and influence on high-temperature creep strength were investigated. In this study, we defined the solution rate R_{sol} ($= (1 - V_{f,e}) \times 100\%$, where $V_{f,e}$ is volume fraction of eutectic γ′ that precipitates in the final solidification zone during casting) as a parameter to reveal the microstructure homogeneity. The R_{sol} values were 71%, 97%, 99%, 100% for solutioning at 1250°C/20 h, 1320°C/5 h, 1320°C/20 h and 1335°C/20 h, respectively. Furthermore, it was confirmed that Re and W segregated in the dendrite core area and γ′ formers whereas Ta and Al segregated in the interdendrite. The magnitude of these segregations decreased as the solution temperature and time increased, and eventually the structure became almost homogeneous for solutioning at 1335°C for 20 hours. Additionally, creep test results indicate that Larson-Miller parameter (LMP) at 800°C–735 MPa, 900°C–392 MPa and 1000°C–245 MPa creep conditions show the same values for $R_{sol} \geq 97\%$. On the other hand, under 1100°C–137 MPa creep condition, LMP decreased as the R_{sol} decreased. A factor analysis of creep rupture properties suggested that the degradation of LMP under 1100°C–137 MPa was caused by the decrease of Re content and γ/γ′ lattice misfit in the interdendritic region.
[doi:10.2320/matertrans.MT-M2024118]

(Received August 9, 2024; Accepted August 21, 2024; Published October 25, 2024)

Keywords: *Ni-base superalloy, single crystal, solution heat treatment, segregation, high-temperature creep strength*

1. Introduction

γ′ precipitation-strengthened Ni-base superalloys (hereafter referred to as Ni-base superalloys) are alloys strengthened by precipitating Ni_3Al-type ($L1_2$ structure) intermetallic compounds (γ′ phase) in the γ phase (FCC structure), a Ni solid solution, and are used as high temperature components in jet engines and gas turbine engines for power generation. Increasing the combustion gas temperature is an effective way to improve the efficiency of gas turbine engines. To achieve this, Ni-base superalloys are required to have excellent high-temperature creep strength, etc. Recently, single-crystal superalloys have been used as turbine blades for power generation gas turbine [1]. The use of computer-aided alloy design methods [2–5] has led to rapid improvements in alloy components, and many of the latest Ni-base superalloys [6, 7] have been proposed that contain elements with high melting points, such as Re and Ru. In the latest aircraft engine turbines, 3rd-generation superalloys such as CMSX-4 and CMSX-10K developed by Cannon-Muskegon [8, 9] are being utilized for turbine blade. The TMS-238 alloy [10], a 6th-generation superalloy developed and proposed by National Institute for Materials Science (NIMS), is attracting attention both domestically and internationally as an alloy that offers superior service temperature and oxidation resistance.

Solution heat treatment is an important process in the manufacture of Ni-base single crystal superalloys. The solidification microstructure of a multi-components Ni-base superalloy usually exhibits a dendrite microstructure with strong elemental segregation, and the alloying element concentrations in the dendrite core (hereinafter referred to as 'd area') and interdendrite region (hereinafter referred to as 'id area') are significantly different. In addition, eutectic γ′ phase and coarse γ′ phase precipitate in the id area corresponding to the final solidification section. In general, it is known that the high-temperature creep strength of Ni-base superalloys is significantly affected by the precipitation morphology of the γ′ phase [11, 12]. It is important to eliminate elemental segregation and eutectic γ′ phase by solution heat treatment in the γ single-phase temperature region before aging heat treatment in order to precipitate fine cuboidal γ′ phase uniformly in the γ matrix phase.

Since the γ′ solvus temperature, eutectic temperature, and diffusion rate of the constituent elements differ depending on the alloy composition, the solution heat treatment conditions must be optimized for each alloy [13, 14]. The latest multi-components alloys tend to have high the γ′ solvus temperatures and low eutectic temperatures, so the process window for solution heat treatment is narrow. Table 1 shows the solution heat treatment conditions for CMSX-4, CMSX-4Plus, CMSX-10K, and TMS-238 [15]. The 3rd-generation superalloys such as CMSX-4Plus and CMSX-10K require significantly complicated heat treatment processes, including eight and ten steps with detailed temperature increase, respectively, to avoid partial melting due to the narrow process window, leading to the high heat treatment cost. In contrast, TMS-238 is an alloy with a wide process window and can be fully solution treated at the optimum solution heat treatment conditions of 1345°C/20 h, making it a relatively productive alloy. However, there is a high need for further process cost reduction in industry. In the case of TMS-238, there is a demand to find low-cost solution conditions at lower temperatures and in shorter time while maintaining creep properties. For example, if solution heat treatment were possible at approximately 1320°C, which is the final solution

*1This Paper was Originally Published in Japanese in J. Japan Inst. Met. Mater. **87** (2023) 288–297.
*2Corresponding author, E-mail: OSADA.Toshio@nims.go.jp

Table 1 Solution heat treatment and aging conditions of CMSX-4, CMSX-4Plus, CMSX-10K and TMS-238.

Alloy	Solution treatment condition	Aging condition
CMSX-4	1277 ºC/2 h +1288 ºC/2 h +1296 ºC/3 h +1304 ºC/3 h +1313 ºC/2 h +1316 ºC/2 h +1318 ºC/2 h +1321 ºC/2 h/GFC	1140 ºC/6 h/AQ +871 ºC/20 h/AQ
CMSX-4 Plus	1313 ºC/2 h +1318 ºC/2 h +1324 ºC/6 h +1335 ºC/6 h/GFC	1163 ºC/6 h/AQ +871 ºC/20 h/AQ
CMSX-10K	1315 ºC/1 h +1329 ºC/2 h +1335 ºC/2 h +1340 ºC/2 h +1346 ºC/2 h +1352 ºC/3 h +1357 ºC/3 h +1360 ºC/5 h +1363 ºC/10 h +1365 ºC/15 h/GFC	1152 ºC/6 h/AQ +871 ºC/24 h/AQ
TMS-238	1300 ºC/1h +1310 ºC/1h +1335 ºC/3h +1345 ºC/20h /GFC	1150 ºC/2 h/AQ +870 ºC/20 h/AQ

Table 2 Nominal and analytical compositions of TMS-238.

	Chemical composition (wt%, Ni balanced)								
	Co	Cr	Mo	W	Al	Ta	Re	Ru	Hf
Nominal	6.5	4.6	1.1	4.0	5.9	7.6	6.4	5.0	0.1
Analyzed	6.4	4.5	1.1	4.0	5.9	7.7	6.4	5.0	0.1

temperature of CMSX-4, TMS-238 can be expected to be applied to a wider range of parts.

Although there are limited studies on the effect of alloying element segregation on dendrite microstructures (hereafter referred to as dendritic segregation), for example, A. Epishin *et al.* [16] reported residual stress due to segregation causes heterogeneity in the lattice between γ–γ′ phases, which affects primary creep strength for CMSX-4. Meanwhile, K.B. Povarova *et al.* [17] reported the degree of dendritic segregation of alloying elements including Re after solution annealing at 1290°C for 2 h to 10 h using γ′-Ni_3Al-based Re-doped alloys with γ + γ′ two-phase structure. Further, Y. Han *et al.* [18] reported influence of dendrite and Cr homogenization on carbide precipitation morphology in Cr-Mo-V steel. However, the relationship between solution heat treatment conditions and mechanical strength of the latest Ni-base single-crystal superalloys is not clear in any of these reports.

The purpose of this study was to investigate the effects of solution heat treatment conditions on high-temperature creep properties of a 6th-generation Ni-base single crystal superalloy TMS-238 containing Re and Ru. In particular, the effects of solution heat treatment conditions on the degree of homogenization of dendritic segregation and the disappearance of eutectic γ′ and coarse γ′ phases were quantified, and their effects on the creep deformation mechanism were investigated. The solution heat treatment conditions at low temperatures or short times are discussed.

2. Experimental Procedure

2.1 Materials and specimens

Using a TMS-238 alloy master ingot, a single-crystal round bar 130 mm long and 10.5 mm in diameter was cast by the pulling-down method in a directional solidification furnace. The casting conditions were as follows: molten metal temperature was at 1600°C, casting temperature was at 1550°C, and the pulling-down speed was 200 mm/h. The nominal composition and analytical composition of the cast round bar are shown in Table 2. Here, compositional analysis was performed using an ICP optical emission spectrometer (ICP-OES: Aligent ICP-OES 720-ES). Although the analyzed composition of the cast round bar was almost equivalent to the nominal composition [10], the Cr and Co contents were 0.1 wt% lower and the Ta content was 0.1 wt% higher. Therefore, it should be noted that the single-crystal samples used in this study have slightly lower microstructural stability [19] than single-crystal samples of nominal composition and are prone to precipitation of the topologically closed pack (TCP) phase [20] during creep. The crystal orientation of the cast single-crystal round bars were measured in the solidification direction by the back-reflection Laue method. In this study, the bars with an orientation difference of 4° or less between ⟨100⟩ growth orientation were selected for solution heat treatment and creep tests.

2.2 Heat treatment and creep test conditions

The selected single-crystal round bars were solution heat treated at 1250°C–20 h, 1300°C–20 h, 1320°C–5 h, 1320°C–20 h, and 1335°C–20 h. The γ′ solvus temperature calculated from compositions of round bar, which were shown in Table 2, by the Alloy Design Program (ADP) [3–5] is 1307°C. This confirms that the heat treatment conditions cover a wide range from the γ/γ′ two phase temperature to just below the eutectic temperature. In solution heat treatment above 1320°C, heat treatment with stepwise temperature increase were performed as shown in Table 3 to avoid partial melting at the id area. In addition, all solution heat treated specimens were subjected to a two-step aging heat treatment of 1150°C–2 h + 870°C–20 h. Creep specimens with a gauge length of 22 mm and a parallel diameter of 4 mm were prepared from the aged specimens in accordance with JIS-

Table 3 Solution heat treatment conditions of TMS-238 in this study.

Cond.	Temperature(ºC) and hold time(h)
As cast	
1250C-20h	1250ºC/20h -> WQ
1300C-20h	1300ºC/20h -> WQ
1320C-20h	1300ºC/0.5h -> 1320ºC/20h -> WQ
1335C-20h	1300ºC/0.5h -> 1320ºC/0.5h -> 1335ºC/20h -> WQ
1320C-5h	1300ºC/0.5h -> 1320ºC/5h -> WQ

Z2271. Creep tests were conducted under four conditions: 800°C–735 MPa, 900°C–392 MPa, 1000°C–245 MPa, and 1100°C–137 MPa.

2.3 Evaluation of microsegregation and microstructure

Dendritic segregation and solution rate R_{sol} were evaluated for six samples including as-cast material. In this study, the degree of dendritic segregation was quantified by defining a microsegregation coefficient, *SR*, as follows:

$$SR = \frac{C_i^d}{C_i^{id}} \quad (1)$$

where C_i^d is the concentration of *i* element in the d area (wt%) and C_i^{id} is the concentration of *i* element in the id area (wt%). Each element concentration was measured using an Electron Probe Micro Analyzer (EPMA: Shimadzu EPMA-1610). The average value of concentration at five points in the d and id area, respectively, was used.

The degree of homogenization by solution heat treatment is often evaluated by the amount of residual coarse γ′ phase formed during the solidification process [21]. Therefore, the solution rate R_{sol} is defined as follows:

$$R_{sol} = (1 - V_{f,e}) \times 100\% \quad (2)$$

where $V_{f,e}$ are the volume fractions of the eutectic γ′ and coarse γ′ phases remaining in the id area after solution heat treatment. Field Emission Scanning Electron Microscope (FE-SEM: Zeiss Gemini 300) was used for evaluation. Since the solidified structure of the alloy used in this study has a primary dendrite arm spacing of approximately 200 mm, the volume fraction of the coarse γ′ phase was measured on a 2 × 2 mm observation region at the center of the sample, in order to evaluate a sufficient amount of γ′ phase, and determined the values of R_{sol}. Further, the initial microstructure before creep and deformed microstructures after creep were observed in the {100} plane corresponding to the dendritic growth and in the {100} plane perpendicular to the growth direction, respectively. The obtained SEM photographs were analyzed using ImageJ [22] to quantify the γ′ volume fraction and γ′ size in the initial microstructure.

3. Results

3.1 Microstructure and microsegregation homogenization by solution heat treatment

Figure 1 shows the backscattered electron image (BEI) of the as-cast specimens and the distribution of Re, W, Al, Ta, and Ni. The image was observed from the ⟨100⟩ direction.

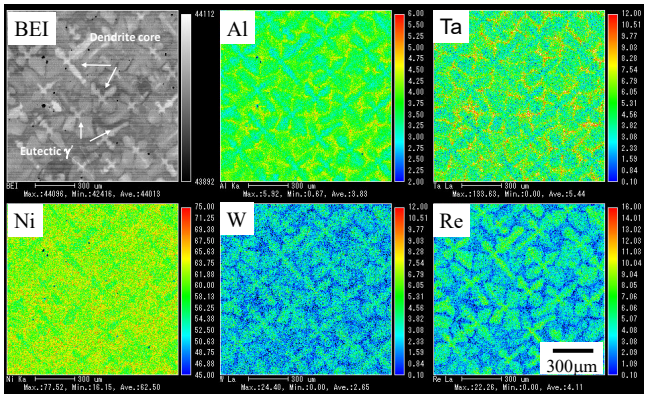

Fig. 1 Elemental segregation of alloying elements in as cast TMS-238 alloy.

The dendritic structure of the as-cast specimen can be clearly seen in the image, elements with high melting point such as Re and W were concentrated in the d area, while Al and Ta are strongly segregated in the id area, indicating the strong segregation of alloying elements. In addition, a large amount of eutectic γ′ phase, which precipitates in the final solidification zone, was observed in the id area of the as-cast specimen. Figure 2(a)–(f) shows the BEI images for as cast specimen and solution heat treated specimens. Here, the white areas correspond to the d areas and the dark areas to the id areas. The growth of secondary dendrite arms from the dendrite core in the ⟨100⟩ direction up, down, left, and right were observed as white areas. The microsegregation from the d areas to id areas observed in the as-cast specimen is homogenized as the solution heat treatment temperature and time increase, resulting in the contrast difference in the BEI image decreases. The volume fraction of the eutectic γ′ phase $f_{v,e}$ was 0.32 in the as-cast specimen, and decreased as the solution temperature and time increased. Table 4 shows the solution rate R_{sol} for each of these solution heat treated specimens. The volume fraction of the eutectic γ′ phase in the specimens solution heat treated at 1250°C–20 h, 1300°C–20 h, 1320°C–5 h, 1320°C–20 h, and 1335°C–20 h determined by SEM observation were 0.29 ($R_{sol} = 71\%$), 0.08 ($R_{sol} = 92\%$), 0.03 ($R_{sol} = 97\%$), and 0.01 ($R_{sol} = 99\%$), and 0.00 ($R_{sol} = 100\%$) respectively. Table 4 shows the EPMA analytical results (wt%) and segregation coefficients *SR* of alloying elements in the d area and id area for the various solution heat treated specimens. Here, the EPMA analysis values for the id area correspond to the composition values for the vicinity of the eutectic γ′ phase, avoiding it. As shown in Table 4, Co, Cr, Mo, W, Re, and Ru, which are γ formers, are concentrated in d area and Al and Ta which are γ′ formers are concentrated id area in the as-cast specimen, indicating that $SR > 1$ for the γ formers and $SR < 1$ for the γ′ formers. Meanwhile, it was confirmed that the segregation coefficient approaches $SR = 1$, since all elements (Co, Cr, Mo, W, Al, Ta, Re, Ru, and Hf) diffuse between the d area and id area as the solution temperature and solution time increases.

Figure 3(a) and (b) show the effect of solution temperature and time, respectively, on the segregation coefficient *SR* of Re, W, Ta, and Al, which have strong segregation tendency in

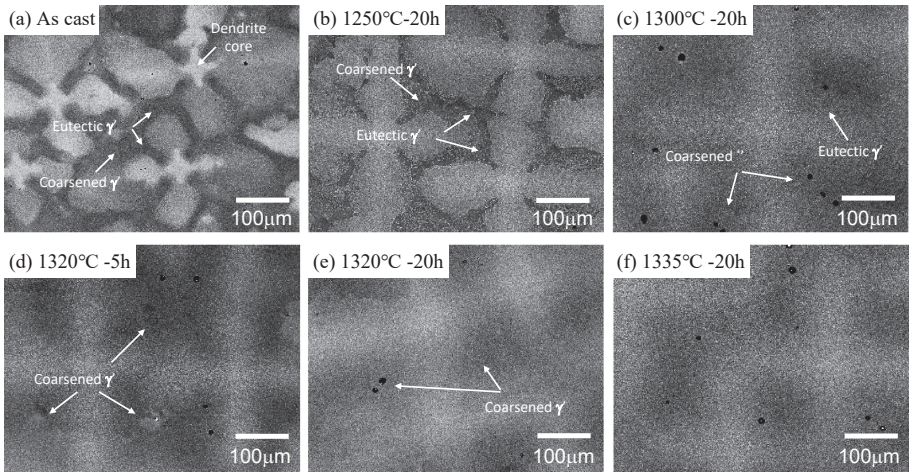

Fig. 2 BEI images of TMS-238: (a) as cast specimen and specimens heat treated for (b) 1250°C–20 h, (c) 1300°C–20 h, (d) 1320°C–5 h, (e) 1320°C–20 h and (f) 1335°C–20 h.

Table 4 Analytical compositions of dendrite core (d) and interdendritic region (id) for each solution heat treatment condition.

Solution teatment condition		Analitical compositions (wt%, Ni;balanced)									Solution rate R_{sol}(%)
		Re	W	Al	Ta	Co	Cr	Mo	Ru	Hf	
As cast	d	11.45 ± 0.04	5.71 ± 0.03	4.80 ± 0.03	5.37 ± 0.32	6.60 ± 0.14	4.59 ± 0.09	1.09 ± 0.00	5.30 ± 0.16	0.15 ± 0.15	68
	id	1.70 ± 0.09	1.86 ± 0.15	7.35 ± 0.05	13.23 ± 0.01	5.07 ± 0.03	2.84 ± 0.06	0.73 ± 0.04	4.37 ± 0.14	0.20 ± 0.01	
	SR	6.73 ± 0.35	3.07 ± 0.24	0.65 ± 0.01	0.41 ± 0.02	1.30 ± 0.03	1.62 ± 0.05	1.49 ± 0.08	1.21 ± 0.05	0.76 ± 0.74	
1250°C-20h	d	9.94 ± 0.03	4.86 ± 0.14	4.93 ± 0.21	5.77 ± 0.25	6.83 ± 0.01	5.56 ± 0.23	1.35 ± 0.15	5.49 ± 0.11	0.06 ± 0.06	71
	id	1.63 ± 0.21	2.59 ± 0.11	7.48 ± 0.05	11.85 ± 0.15	4.95 ± 0.09	2.34 ± 0.16	0.64 ± 0.09	3.94 ± 0.14	0.23 ± 0.01	
	SR	6.09 ± 0.77	1.87 ± 0.10	0.66 ± 0.03	0.49 ± 0.02	1.38 ± 0.03	2.38 ± 0.19	2.10 ± 0.37	1.39 ± 0.06	0.26 ± 0.27	
1300°C-20h	d	9.65 ± 0.45	4.60 ± 0.16	4.80 ± 0.04	6.03 ± 0.03	6.99 ± 0.02	5.58 ± 0.30	1.38 ± 0.18	5.75 ± 0.12	0.01 ± 0.02	92
	id	3.35 ± 0.45	3.50 ± 0.27	6.54 ± 0.17	8.79 ± 0.41	5.69 ± 0.20	3.69 ± 0.44	0.94 ± 0.05	4.51 ± 0.18	0.17 ± 0.02	
	SR	2.88 ± 0.41	1.31 ± 0.11	0.73 ± 0.02	0.69 ± 0.03	1.23 ± 0.04	1.51 ± 0.20	1.46 ± 0.21	1.27 ± 0.06	0.23 ± 0.10	
1320°C-5h	d	10.13 ± 0.19	4.70 ± 0.10	5.00 ± 0.13	6.47 ± 0.04	6.73 ± 0.14	5.04 ± 0.04	1.23 ± 0.06	5.68 ± 0.06	0.10 ± 0.11	97
	id	3.57 ± 0.31	3.25 ± 0.14	6.43 ± 0.03	8.88 ± 0.14	5.90 ± 0.03	3.99 ± 0.04	1.16 ± 0.08	5.35 ± 0.77	0.26 ± 0.10	
	SR	2.84 ± 0.26	1.45 ± 0.07	0.78 ± 0.02	0.73 ± 0.01	1.14 ± 0.02	1.26 ± 0.02	1.07 ± 0.09	1.06 ± 0.15	0.38 ± 0.43	
1320°C-20h	d	7.74 ± 0.01	4.20 ± 0.10	5.65 ± 0.01	7.35 ± 0.00	6.29 ± 0.05	4.53 ± 0.01	1.11 ± 0.10	5.04 ± 0.10	0.11 ± 0.01	99
	id	5.10 ± 0.09	3.68 ± 0.34	6.04 ± 0.01	8.29 ± 0.09	6.30 ± 0.10	4.39 ± 0.18	1.05 ± 0.03	4.72 ± 0.02	0.16 ± 0.03	
	SR	1.52 ± 0.03	1.14 ± 0.11	0.93 ± 0.00	0.89 ± 0.01	1.00 ± 0.02	1.03 ± 0.04	1.06 ± 0.10	1.07 ± 0.02	0.71 ± 0.15	
1335°C-20h	d	7.44 ± 0.02	4.02 ± 0.10	5.70 ± 0.02	7.34 ± 0.24	6.45 ± 0.10	4.55 ± 0.05	1.12 ± 0.07	5.00 ± 0.10	0.25 ± 0.08	100
	id	5.61 ± 0.05	4.11 ± 0.22	5.60 ± 0.04	7.94 ± 0.06	6.35 ± 0.07	4.73 ± 0.08	1.07 ± 0.06	5.44 ± 0.10	0.08 ± 0.03	
	SR	1.33 ± 0.01	0.98 ± 0.06	1.02 ± 0.01	0.92 ± 0.03	1.02 ± 0.02	0.96 ± 0.02	1.05 ± 0.09	0.92 ± 0.03	3.14 ± 1.59	

the d and id areas. As shown in Fig. 3(a), the *SR* values of Re and W in the as cast specimen were positive ($SR = 6.73$ and $SR = 3.07$, respectively), because these elements are segregated in the d area, which is the initial solidification zone, while the *SR* values of Ta and Al, which are the γ′ formers, were negative ($SR = 0.41$ and $SR = 0.65$, respectively) because these elements are segregated in the id area, which is the final solidification zone. As a result of decrease in the difference in elements concentration between the d and id areas, the values of segregation coefficients for all alloying elements approach to $SR = 1$ with increasing solution temperature. The conditions at 1335°C for 20 h, where homogenization was most advanced in this study, showed $SR = 1.33$ and 0.92 for Re and Ta with low diffusion coefficient, while $SR = 1$ for almost all other alloying elements, confirming that the conditions under which alloying elements are sufficiently homogenized. Figure 3(b) shows that the segregation coefficients *SR* for Re, W, Ta, and Al decrease rapidly up to 5 h of heat treatment at a solution temperature of 1320°C, and then gradually approach 1. However, Ta with a lowest diffusion coefficient among the γ′ formers showed $SR = 0.69$ and $C_{id} = 8.88$ wt% even after 5 h of heat treatment, indicating that the concentration of Ta in the id area was still high.

Figure 3(c) shows the relationship between the solution rate R_{sol} of various solution-treated specimens and the solidus temperature and γ′ solvus temperature of compositions in the id area. Here the solidus and γ′ solvus temperature were calculated by ADP from compositions of the id area with γ′ formers segregated. The X mark in the figure indicates the solution temperature. As shown in the figure, the γ′ solvus temperatures of specimens heat-treated at 1250°C–20 h ($R_{sol} = 71\%$), 1300°C–20 h ($R_{sol} = 92\%$) and 1320°C–5 h ($R_{sol} = 97\%$) were higher than solution heat treatment

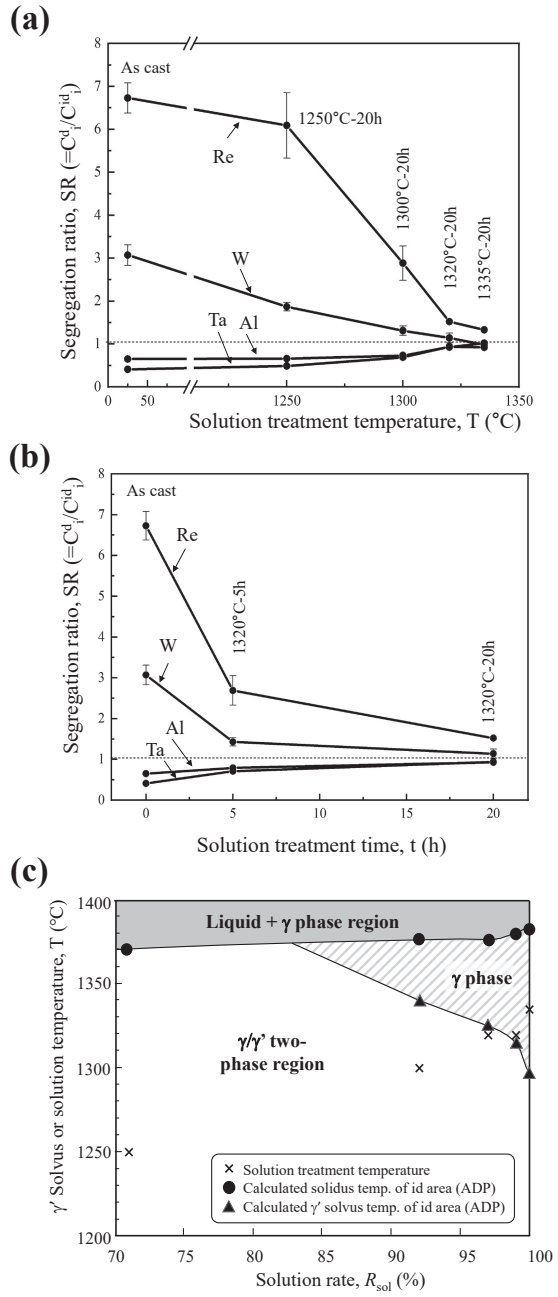

Fig. 3 Change of Segregation ratio SR for alloying elements Re, W, Al, Ta depending on (a) solution treatment temperatures and (b) time. (c) γ′ solvus and solidus temperature calculated from compositions of id area by NIMS–ADP.

temperatures. This confirmed that these heat treatment conditions corresponded to the γ/γ′ two phase temperature region in the id area. However, the γ′ solvus temperature of the specimen heat-treated at 1320°C–5 h was 1326°C, implying that the solution temperature was only 6°C lower than the γ′ solvus temperature. Meanwhile, the γ′ solvus temperatures of specimens heat-treated at 1320°C–20 h ($R_{sol} = 99\%$) and 1335°C–20 h ($R_{sol} = 100\%$) were 1316°C and 1297°C, respectively, indicating that the id area reached the γ single-phase temperature region after solution treatment.

The above-mentioned residual eutectic γ′ phase and differences in the concentrations of various elements in the d and id areas could have a significant effect on the creep life of the aged specimens as described below.

3.2 Effect of solution heat treatment on microstructure of aged specimens

Figures 4(a)–(d) show the microstructure of the aged specimens before the creep test. The observed images correspond to the microstructure of the {100} plane perpendicular to the ⟨100⟩ growth direction. Further, enlarged images showing microstructure of d and id area were also shown in the figures. In the aged specimen solution heat-treated at 1250°C for 20 h, there are many coarse γ′ phases in addition to a significantly coarse eutectic γ′ phase in the id area. The coarse γ′ are the precipitates that grew at 1250°C, since the conditions of 1250°C–20 h corresponds to the γ/γ′ two phase temperature region for the composition of the id area, as shown in Fig. 3(c). Meanwhile, the very fine γ′ phase is considered to be the γ′ phase precipitated by aging heat treatment at 870°C. Further, a large amount of fine γ′ phase precipitated in d area, showing a γ/γ′ two phase structure. On the other hand, the eutectic γ′ phase remained in the id area of the specimen solution heat-treated at 1320°C for 5 h, while the coarse γ′ phase was slight. This is because the solution temperature corresponds to the γ/γ′ two phase region, but very close to the γ′ solvus temperature (1326°C), resulting in the limited area of coarse growth of the γ′ phase. In addition, most of the area other than the eutectic γ′ phase and the coarse γ′ phase formed a two-phase structure with relatively uniform fine γ′ precipitates. On the other hand, in the 1320°C–20 h and 1335°C–20 h solution heat-treated specimens with $R_{sol} = 99$–100%, two phase structure, in which the fine γ′ phase was uniformly precipitated in both the d and id area, formed, since the solution heat treatment condition is temperature region of γ single phase over the entire specimen.

Figure 5(a) and (b) show the γ′ volume fraction and size in the d and id area, respectively, analyzed from SEM images of various aged specimens. It was found that the γ′ volume fraction and size of the d area increased and the γ′ volume fraction and size of the id area decreased with increasing solution temperature and time (or solution rate R_{sol}). Further, the volume fraction and size of the d area and the id area of the specimen solution heat-treated at 1335°C–20 h ($R_{sol} = 100\%$) were almost identical, and $V_f = 73\%$ and $d = 325$–330 nm, respectively. The volume fraction is the almost equals to that calculated by ADP using the compositions shown in Table 2, indicating that the dendritic segregation was eliminated and sufficiently homogenized at 1335°C–20 h. At the same time, it also was confirmed that the volume fraction of γ′ can be accurately predicted by ADP. On the other hand, the volume fraction of the aged specimens under the conditions of low solution rate is large in the id area containing a large amount of γ′ formers, such as Al and Ta, while the volume fraction is low in the d area containing less amount of Al and Ta. Meanwhile, 1250°C–20 h ($R_{sol} = 71\%$) and 1320°C–5 h ($R_{sol} = 97\%$) heat-treated specimens have a much larger γ′ size in the id area than in the other conditions. This is due to solution heat treatment conditions is within the γ/γ′ two phase temperature region.

In addition to the residual eutectic γ′ phase and the differences in the concentrations of alloying elements in the d and id areas, as mentioned in section 3.1, the differences in volume fraction and size of γ′ in the d and id area are also

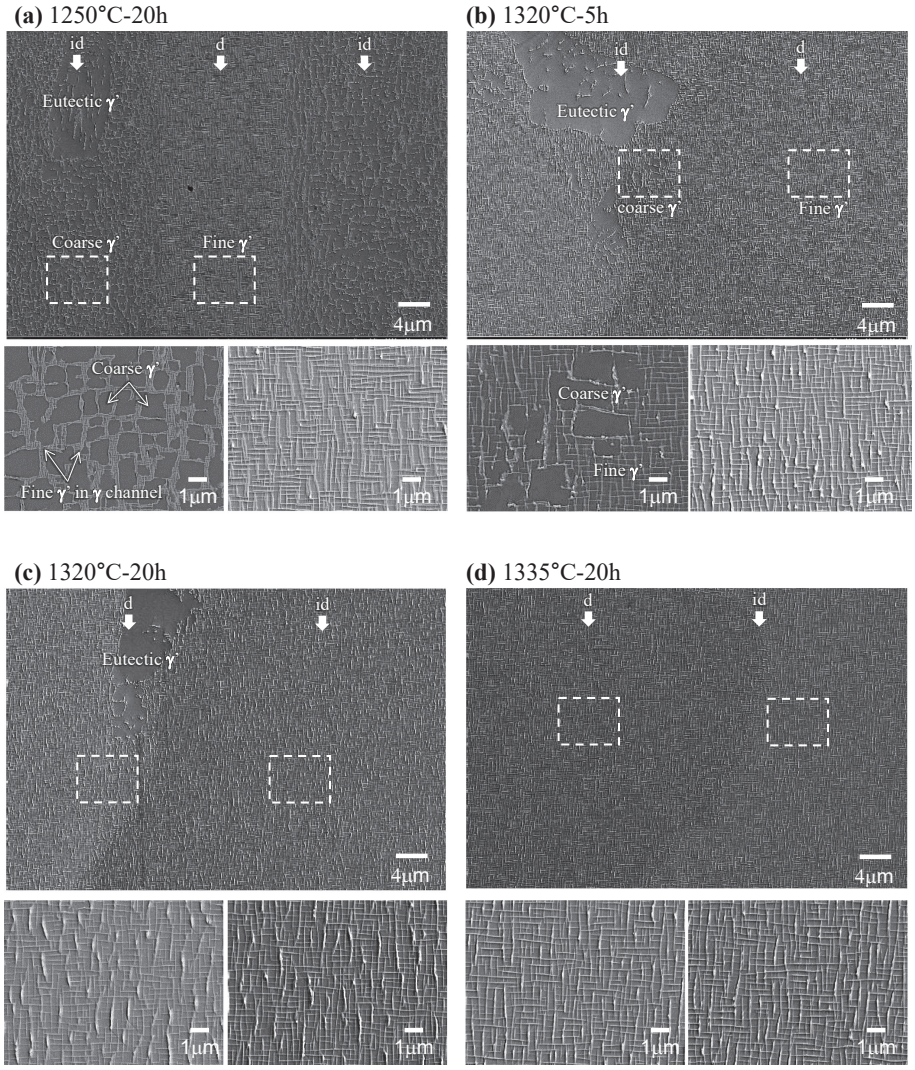

Fig. 4 Initial microstructures of specimens heat treated for (a) 1250°C–20 h, (b) 1320°C–5 h, (c) 1320°C–20 h and (d) 1335°C–20 h before creep test.

considered to have a significant effect on the creep life of various aged specimens, as described below.

3.3 Effect of solution heat treatment conditions on high-temperature creep life

Figure 6 shows the creep curves of various aged specimen at (a) 800°C–735 MPa, (b) 900°C–392 MPa, (c) 1000°C–245 MPa and (d) 1100°C–137 MPa. The relationship between the applied stress and the Larson-Miller parameter (LMP = $T \cdot (20 + \log t_r)$) is summarized in Fig. 7. As shown in Fig. 7, under all creep conditions, the LMP value of the aged specimen solution heat-treated at 1250°C–20 h, in which solution rate R_{sol} is the lowest and many eutectic γ' phases and coarse γ' phases remain, was lower than that of aged specimen solution heat-treated at 1335°C–20 h. Thus, it is confirmed that the heterogeneous microstructure significantly reduced the creep lifetime. The decrease in LMP value became more pronounced with increasing creep temperature. Especially at 1100°C–137 MPa, which is a high temperature low stress creep condition, the LMP value was −1.1 lower than that of the aged specimen solution heat-treated at 1335°C–20 h. This value corresponds to a significant decrease of −47°C for temperature capability (temperature for 1000 h creep rapture life at 137 MPa), implying that optimization of solution heat treatment conditions is key importance to ensure the performance of the latest 6th-generation single-crystal superalloy TMS-238. On the other hand, it was also confirmed that there is no significant difference in LMP values under the 800°C–735 MPa, 900°C–392 MPa, and 1000°C–245 MPa creep conditions when R_{sol} is 97% or higher (solution temperature ≥ 1320°C). However, under 1100°C–137 MPa conditions, which is a high-temperature low-stress region, LMP was found to decrease significantly as R_{sol} decreased. Note that TMS-238 showed better creep life properties than the commercial alloy CMSX-4 (3rd-generation alloy) under all creep conditions, even under the 1250°C–20 h solution heat treatment condition.

Figures 8 and 9 show Secondary Electron Images (SEI) of the microstructure after the creep test at each creep condition. All the images were taken at position approximately 1 mm away from the extensometer limbs. As shown in Fig. 8(a), the microstructure after the 800°C–735 MPa creep test was not significantly rafted, and the shape, size and volume fraction of the γ' phase were similar to the initial

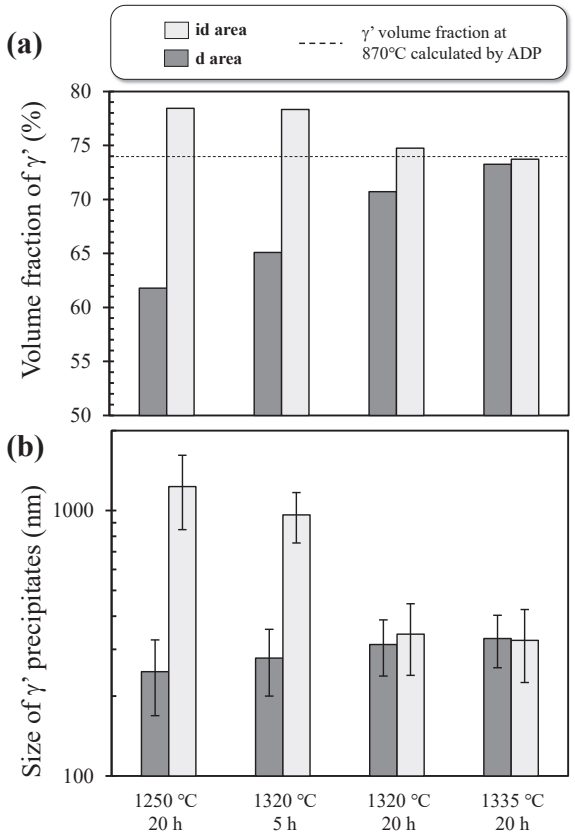

Fig. 5 (a) γ′ volume fraction and (b) size at d and id area in sample solution heat-treated at various conditions.

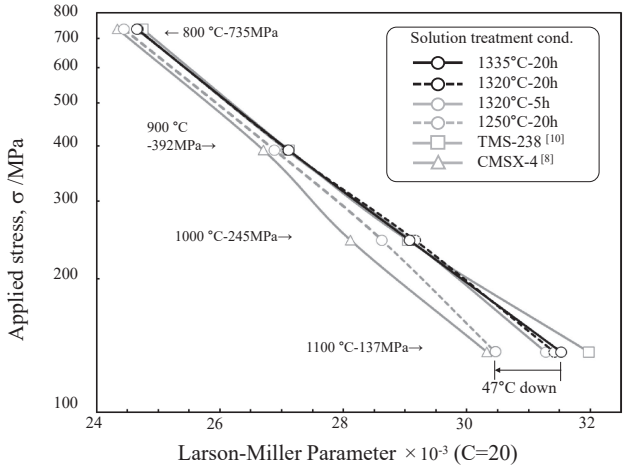

Fig. 7 Larson-Miller plot of creep test results.

microstructure for all aged specimens. This is due to the creep temperature being lower than the aging temperature (870°C), and the volume fraction of γ′ increasing slightly during the creep test. Under the 900°C–392 MPa creep condition, rafting of the γ′ phase progressed over the entire surface of all the aged specimens, except for the id area of the 1250°C–20 h heat-treated specimen, as shown in Fig. 8(b). Meanwhile, fine rafts were formed in the specimens with R_{sol} higher than 97%, and the raft spacing was also significantly fine. On the other hand, precipitation of fine TCP phases growing on the {111} plane was confirmed, especially in d area. Although detailed analysis of TCP was not performed, it was determined that the phase is a Re and Ru-rich P phase, based on thermodynamic calculations of d area compositions and the previous report in literature [20, 23]. As mentioned in section 2.1, the precipitation of the TCP phase is due to the Ta content of the TMS-238 master ingot used in this study being slightly higher than the nominal composition and the

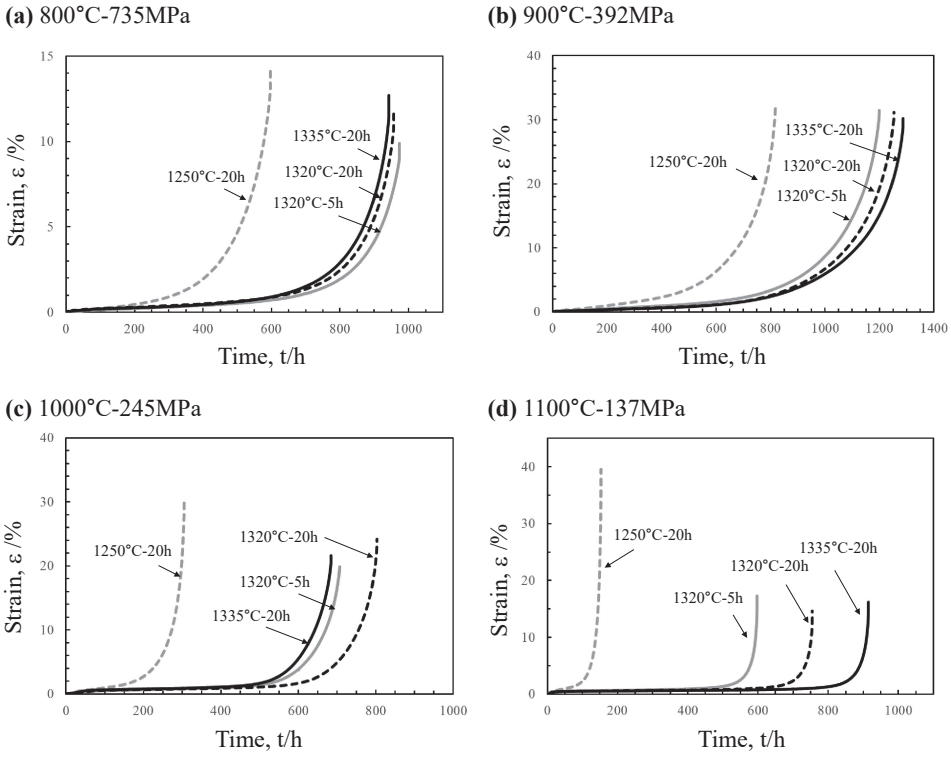

Fig. 6 Creep curves under test conditions of (a) 800°C–735 MPa, (b) 900°C–392 MPa, (c) 1000°C–245 MPa and (d) 1100°C–137 MPa.

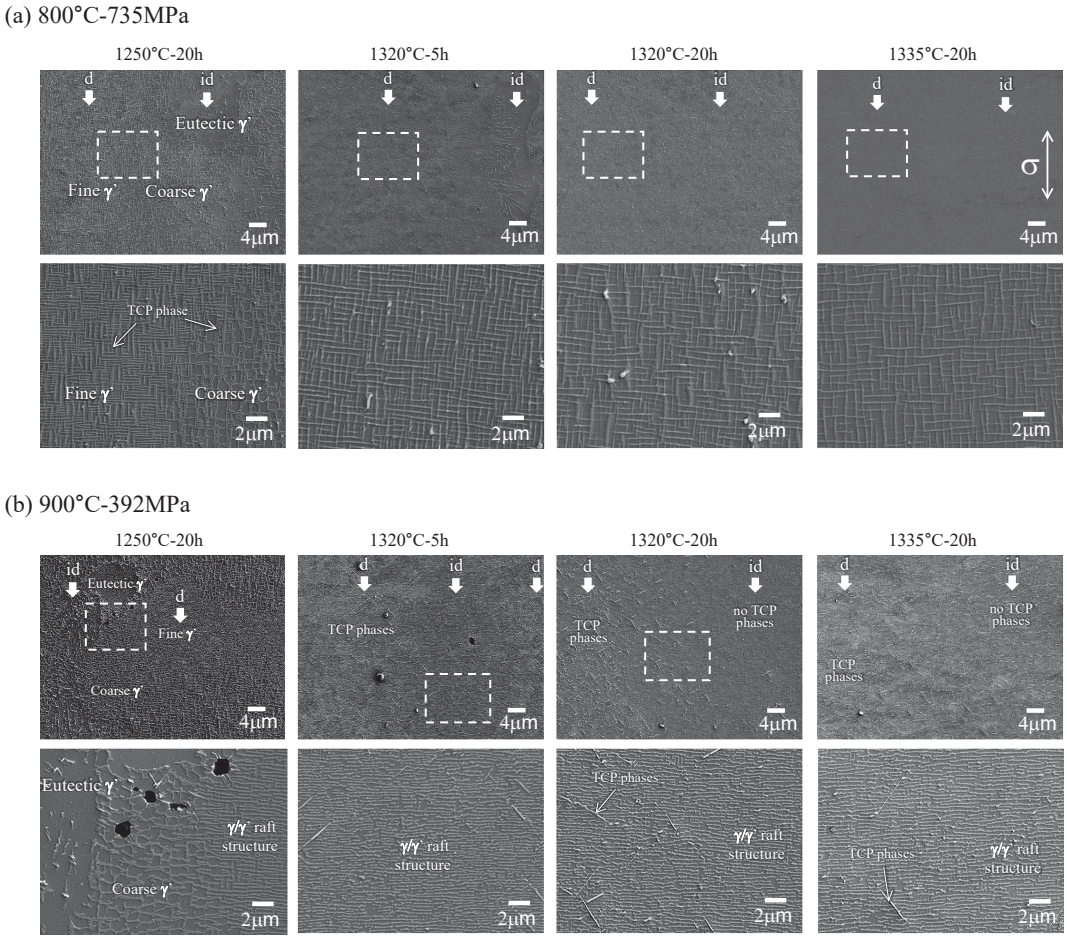

Fig. 8 Microstructures of crept specimens under test conditions of (a) 800°C–735 MPa and (b) 900°C–392 MPa.

enrichment of Re in d area. Figure 9(a) shows the microstructures after the creep test at 1000°C–245 MPa conditions. The microstructures of the various solution heat-treated specimens were almost the same as those under the 900°C–392 MPa creep condition. It was confirmed that the coarse γ' phase remaining in the id area of aged specimen solution heat-treated at 1250°C for 20 h was not rafted. Meanwhile, the TCP phase precipitated in the d area. As shown in Fig. 9(b), under the 1100°C–137 MPa creep condition, rafting of the γ' phase was observed on the entire surface of all solution heat-treated specimens, including the id area of the 1250°C–20 h heat-treated specimen. Further, significantly long TCP phases were observed in several positions in the d area of the specimens with R_{sol} of 97% or more.

4. Discussion

The decrease in solution rate R_{sol} was confirmed to be a factor of residual eutectic γ' phase and large segregation of various element in the d and id areas, leading to microstructural heterogeneity. The creep rupture life of the specimen solution heat-treated at 1250°C–20 h including many remaining eutectic γ' phases and coarse γ' phases were significantly lower than those of the specimens heat-treated at 1335°C–20 h under all creep conditions. On the other hand, there was no significant difference in LMP values under the 800°C–735 MPa, 900°C–392 MPa, and 1000°C–245 MPa creep conditions when R_{sol} was 97% or higher (solution temperature $\geq$ 1320°C). However, under the 1100°C–137 MPa condition, which is a high-temperature and low-stress condition, LMP decreased significantly as R_{sol} decreased. Here, we summarize the relationship between solution rate R_{sol} and creep rupture life at 1100°C–137 MPa using ADP. Although ADP is a prediction program developed to predict creep rupture life from the alloy compositions of fully solutioned single-crystal superalloys, the program could be useful to qualitatively discuss creep properties of the d and id area of the specimen with the inhomogeneous microstructure, calculated from the elemental concentrations in the d and id area obtained in this study.

The multiple regression model implemented in ADP [5] is shown below:

$$log\, t_r(T,\sigma) = a_o + \sum a_i X_i(T) + a_j \delta(T) + a_k V_f(T) + a_l V_f^2(T) \quad (3)$$

where t_r is the creep rupture life; T is the creep temperature; and σ is the creep applied stress; $X_i(T)$ is the concentration of i-alloying element in the γ' phase at temperature T; $\delta(T)$ is the γ/γ' lattice misfit ($\delta = (a_{\gamma'} - a_\gamma)/a_\gamma$, abbreviated as misfit) at temperature T; and $V_f(T)$ is the γ' volume fraction at temperature T. In addition, a_o, a_i, a_j, a_k and a_l are multiple regression coefficients determined from the Ni-base superalloy database accumulated in NIMS. Figure 10(a) shows the

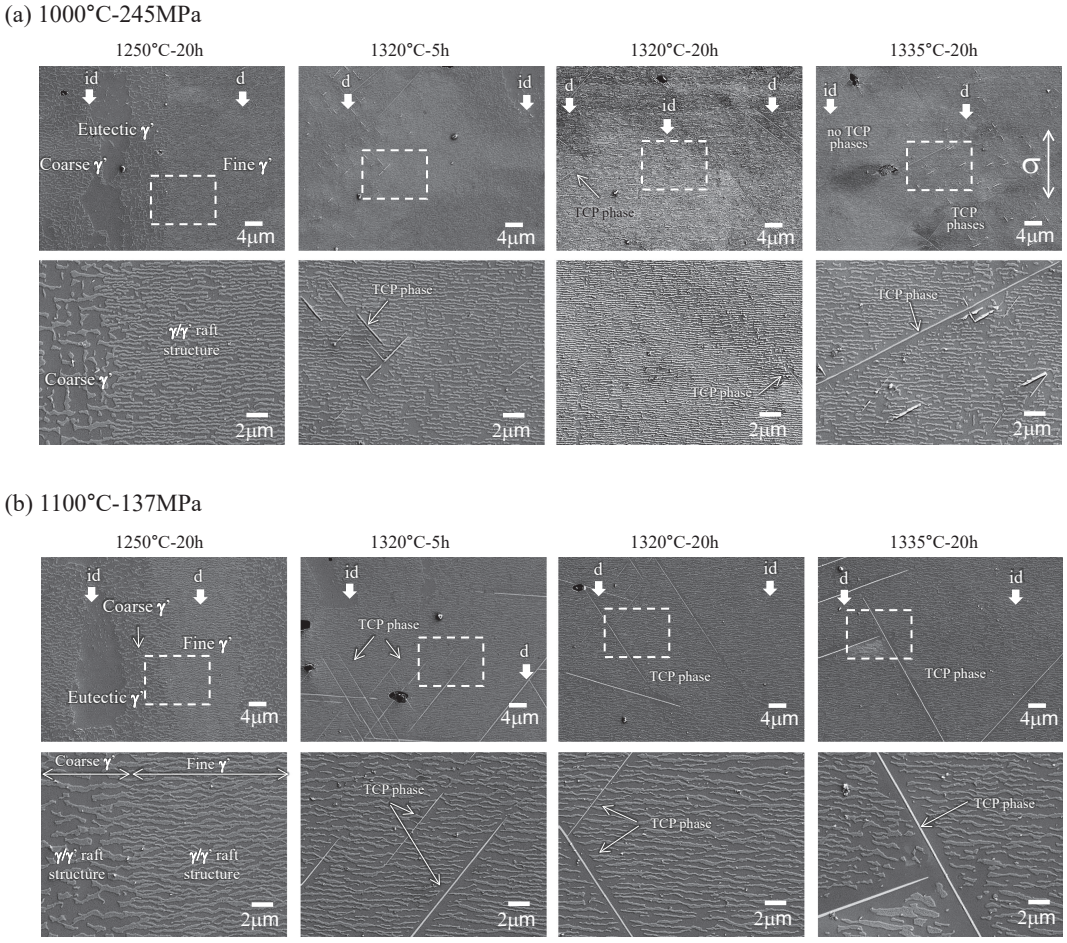

Fig. 9 Microstructures of crept specimens under test conditions of (a) 1000°C–245 MPa and (b) 1100°C–137 MPa.

coefficients a_i (i: W, Ta, Re, Ru) of i-element concentration X_i and the coefficient of misfit a_j obtained under various creep conditions. As shown in the figure, the values of coefficient of Re concentration a_{Re} and the coefficient of misfit a_j are larger than the other contributing factors. This indicates that contribution of Re concentration and misfit to the creep rupture life is significantly large under all creep conditions. Furthermore, the a_{Re} decreases with decreasing creep applied stress (and with increasing creep temperature), while a_j increases significantly in a negative direction with a decrease in creep applied stress. This is due to the significant contribution of the solution strengthening of Re in the low-temperature/high-stress region, while in the high-temperature/low-stress region, in addition to the solution strengthening by Re, the contribution of γ/γ' misfit, which promotes rafting of the γ' phase and strengthening due to the interfacial dislocation network, is also significant [4, 5, 10]. Figure 10(b) shows the LMP values at 1100°C–137 MPa creep conditions predicted from compositions in the d and id areas of various solution heat-treated specimens using the multiple regression model described above. As shown in the figure, the LMP values predicted from the composition of the d area are larger than those of the id area under all solution heat treatment conditions. This indicates that both solid-solution strengthening and misfit contribute significantly to the LMP values because of the Re enrichment in the d area. Therefore, the creep rupture life of the d area tends to be shorter because the Re content decreases with increasing solution temperature. On the other hand, the LMP value of the id area is predicted to be lower than that of the d area, since lower Re content is lower than that of d area, although the id area has a higher volume fraction of the γ' phase, as shown in Fig. 5, due to Ta and Al enrichment. Therefore, the creep rupture life of the id area tends to be longer with increasing Re content as the solution temperature increased. Here, it was confirmed that the measured LMP values were found to be between the LMP values of the d and id areas, and the trend to be in good agreement with the trend of LMP values lowering in the id area. Such a decrease in the creep rupture life, i.e., an increase in creep deformation rate, of the id area with decrease in solution temperature, is expected to promote local deformation in the id area and become a factor for creep void formation and rupture in the id areas. From the above discussion, it can be concluded that the decrease in creep rupture life of the alloy with decreasing solution temperature is mainly due to the increase in the local creep deformation rate in the id area caused by the lack of Re and lower misfit in the id areas.

As described above, it can be concluded that the solution heat treatment for TMS-238, a 6th-generation superalloy, should be conducted at 1320°C or higher for 20 h or longer, which is in the γ/γ' two phase temperature region over the entire the specimen. Note that the dendritic segregation interval (secondary dendrite arm spacing) strongly depends

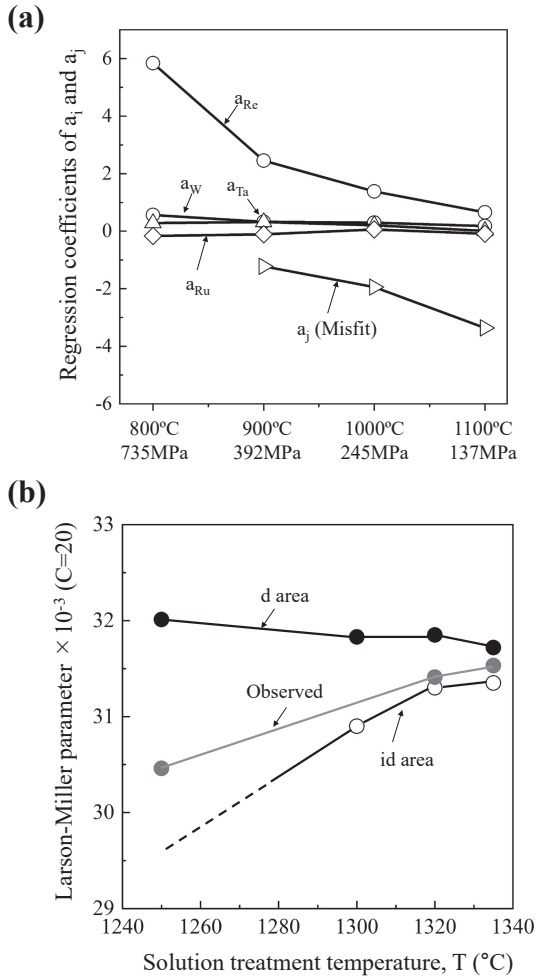

Fig. 10 (a) Regression coefficients of a_i (i: W, Ta, Re, Ru), and a_j (misfit) in the creep rupture life prediction equation (b) predicted creep rupture time under 1100°C/137 MPa creep condition from d and id compositions of various solution heat-treated TMS-238.

on the single crystal casting conditions, especially on the solidification rate [24]. The present results were obtained for dendritic segregation formed under the casting conditions described in section 2.1. When determining solution heat treatment conditions for actual turbine blade-shaped products, it is necessary to set solution heat treatment conditions on the safety side based on a thorough understanding of the solidification conditions at each location on entire turbine blade.

5. Conclusion

Using a 6th-generation Ni-base single-crystal superalloy TMS-238 with Re and Ru additions, systematic comparisons and investigations were conducted on the effects of solution heat treatment conditions on the degree of dendritic segregation and solution rate R_{sol}, and on creep strength at high temperatures. As a result, the following were found:

(1) The eutectic γ′ phase and coarse γ′ phase existed for solution heat-treatment at 1250°C–20 h, similar to the as cast specimen. The eutectic γ′ phase almost disappeared but coarse γ′ phase remained at 1300°C–20 h. The heat treatment at 1320°C–20 h and 1335°C–20 h satisfied the heat treatment conditions in the γ-single phase temperature range over the entire the specimen, resulting in a two-phase structure with uniform and fine g′ phase precipitation in both the d and id areas.

(2) The dendritic segregation coefficient *SR* approaches 1 with increasing solution temperature. *SR* values after solution heat treatment at 1335°C–20 h is 1.33 for Re, 0.92 for Ta, and $SR \cong 1$ for the other alloying elements, indicating that the condition is almost full solution heat treatment conditions.

(3) The 1250°C–20 h solution heat treated specimen showed lower LMP values under all creep conditions. However, it showed superior creep life properties to the commercial single-crystal superalloy CMSX-4 (3rd-generation superalloy).

(4) Under 800°C–735 MPa, 900°C–392 MPa and 1000°C–245 MPa creep conditions, there was no significant difference in LMP values as long as R_{sol} was larger than or equal to 97% (solution temperature ≥ 1320°C).

(5) In the high temperature/low stress region, 1100°C–137 MPa creep condition, the LMP value decreased significantly as R_{sol} decreased.

(6) As the creep prediction results from compositions in the d and id areas of various solution heat-treated specimens using ADP, it is confirmed that the decrease in creep rapture time under 1100°C–137 MPa creep conditions with decreasing solution temperature is associated with a decrease in Re content in the id area and decrease in γ/γ′ misfit.

(7) Solution heat treatment for TMS-238 should be conducted at 1320°C or higher for 20 h or longer, which is in the γ/γ′ two phase temperature range over the entire the specimens.

Acknowledgement

This paper is based on results obtained from a project ‘Aero Engine Materials Development and Evaluation System Infrastructure Development Project’ (JPNP21007) commissioned by the New Energy and Industrial Technology Development Organization (NEDO). We would like to express our deep appreciation to all parties involved.

REFERENCES

[1] H. Harada, T. Yokokawa, K. Kawagishi, T. Kobayashi, Y. Koizumi, M. Sakamoto and M. Yuyama: Materials for High Temperature Turbine Applications: With Actual Practical Use in Mind, J. Gas Turbine Soc. Jpn. **43** (2015) 349–356.

[2] R. Watanabe and T. Kuno: Alloy Design of Nickel-Base Precipitation Hardened Superalloys, Tetsu-to-Hagané **61** (1975) 2274–2294.

[3] H. Harada and M. Yamazaki: Alloy Design for γ′ Precipitation Hardening Nickel-base Superalloys Containing Ti, Ta, and W, Tetsu-to-Hagané **65** (1979) 1059–1068.

[4] T. Yokokawa, H. Harada, Y. Mori, K. Kawagishi, Y. Koizumi, T. Kobayashi, M. Yuyama and S. Suzuki: *Superalloys2016*, ed. by E. Huron, (Seven Springs, Pennsylvania, TMS, 2016) pp. 123–130.

[5] T. Yokokawa, H. Harada, K. Kawagishi, T. Kobayashi, M. Yuyama and Y. Takata: *Superalloys2022*, ed. by S. Tin, (Seven Springs, Pennsylvania, TMS, 2022) pp. 122–130.

[6] K. Kawagishi, A. Sato, T. Kobayashi and H. Harada: Effect of Alloying Elements on the Oxidation Resistance of 4th Generation Ni-

base Single-crystal Superalloys, J. Japan Inst. Metals **69** (2005) 249–252.
[7] K. Kawagishi, A. Sato, T. Kobayashi and H. Harada: Temperature Dependence of Oxidation Properties for 5th Generation Ni-Base Single-Crystal Superalloys, J. Japan Inst. Metals **70** (2006) 686–689.
[8] K. Harris, G.L. Erickson and R.E. Schwer: *Superalloys1984*, ed. by M. Gell, (Champion, Pennsylvania, TMS, 1984) pp. 221–230.
[9] J. Wahl and K. Harris: *Superalloys2016*, ed. by M. Hardy, (Seven Springs, Pennsylvania, TMS, 2016) pp. 25–33. doi:10.1002/9781119075646.ch3.
[10] K. Kawagishi, A.C. Yeh, T. Yokokawa, T. Kobayashi, Y. Koizumi and H. Harada: *Superalloys2012*, ed. by R. Reed, (Seven Springs, Pennsylvania, TMS, 2012) pp. 189–195.
[11] T. Ohno, R. Watanabe and A. Yoshinari: Effect of Aging Heat-treatment Condition on Creep-rupture Strength of Nickel-base Single Crystal Superalloys, Tetsu-to-Hagané **75** (1989) 964–971.
[12] A. Yoshinari: Application and Properties of Ni-based Superalloy Castings, J. JFS **73** (2001) 834–839.
[13] Y. Koizumi, T. Kobayashi, T. Yokokawa, M. Osawa, H. Harada, T. Hino and Y. Yoshioka: Creep Strengths of a Ni-Base Single Crystal Superalloy TMS-82+ and Its Tie-Line Alloys, J. Japan Inst. Metals **67** (2003) 205–208.
[14] T. Takeshita, Y. Murata, N. Miura, Y. Kondo, Y. Tsukada and T. Koyama: Morphology of γ′ Precipitate in NKH71 Nickel Based Superalloy Depending on Heat Treatment, J. Japan Inst. Metals **79** (2015) 203–209.
[15] J. Cormier: *Superalloys2016*, ed. by M. Hardy, (Seven Springs, Pennsylvania, TMS, 2016) pp. 385–394.
[16] A. Epishin, T. Link, U. Brickner, B. Fedelich and P. Portella: *Superalloys2004*, ed. by K. Green, (Seven Springs, Pennsylvania, TMS, 2004) pp. 537–543.
[17] K.B. Povarova, O.A. Bazyleva, A. Drozdov, A.E. Morozov, E.G. Arginbeava and A.V. Antonova, Effect of Heat Treatment on Dendritic Segregation and High-Temperature Strength of Single Crystals of Ni_3Al-Base Rhenium-Alloyed Intermetallic Alloys, Met. Sci. Heat Treat. **60** (2019) 594–601.
[18] Y. Han, C. Li, J. Ren, C. Qui, Y. Zhang and J. Wang: Dendrite Segregation Changes in High Temperature Homogenization Process of As-cast H13 Steel, ISIJ Int. **59** (2019) 1893–1900.
[19] A. Sato, T. Yokokawa, Y. Koizumi, T. Kobayashi and H. Harada: A Factor Analysis of Creep Rupture Properties of Ni-Base Superalloys, J. Japan Inst. Metals **69** (2005) 691–694.
[20] R. Darolia, D.F. Lahrmanand and R.D. Field: *Superalloys 1988*, ed. by D.H. Duhl, (Champion, Pennsylvania, TMS, 1988) pp. 255–264.
[21] G.E. Fuchs: Solution heat treatment response of a third generation single crystal Ni-base superalloy, Mater. Sci. Eng. A **300** (2001) 52–60.
[22] A public domain Java image processing program, National Institutes of Health (NIH), https://imagej.net/ij/index.html.
[23] N. Matan, D.C. Cox, C.F.M. Rae and R.C. Reed: On the kinetics of rafting in CMSX-4 superalloy single crystals, Acta Mater. **47** (1999) 2031–2045.
[24] T. Hatayama, Y. Natsume and K. Ohsasa: Evaluation of Dendrite Structure in Alloys, Tetsu-to-Hagané **103** (2017) 695–702.